Surface related and intrinsic exciton recombination dynamics in ZnO nanoparticles synthesized by a sol-gel method

Hsu-Cheng Hsu, Hsin-Ying Huang, Martin Eriksson, Tsen-Fang Dai and Per-Olof Holtz

Original Publication:

Hsu-Cheng Hsu, Hsin-Ying Huang, Martin Eriksson, Tsen-Fang Dai and Per-Olof Holtz, Surface related and intrinsic exciton recombination dynamics in ZnO nanoparticles synthesized by a sol-gel method, 2013, Applied Physics Letters, (102), 1, 013109.
http://dx.doi.org/10.1063/1.4774002

Surface related and intrinsic exciton recombination dynamics in ZnO nanoparticles synthesized by a sol-gel method

Hsu-Cheng Hsu,[1,2,3,a)] Hsin-Ying Huang,[1] Martin O. Eriksson,[4] Tsen-Fang Dai,[1] and Per-Olof Holtz[4]
[1]*Department of Photonics, National Cheng Kung University, 701 Tainan, Taiwan*
[2]*Advanced Optoelectronic Technology Center, National Cheng Kung University, 701 Tainan, Taiwan*
[3]*Research Center for Energy Technology and Strategy, National Cheng Kung University, Tainan 701, Taiwan*
[4]*Department of Physics, Chemistry, and Biology (IFM), Linköping University, S-58183 Linköping, Sweden*

(Received 13 November 2012; accepted 17 December 2012; published online 8 January 2013)

ZnO nanoparticles with controlled sizes produced by a sol-gel method are studied by means of time-integrated as well as time-resolved photoluminescence (TRPL) spectroscopy. Room-temperature photoluminescence spectra show a blueshift of the excitonic emission with the decreasing particle size, which is attributed to the quantum confinement effect. The temperature dependence of the exciton lifetimes deduced from the TRPL results contains two components: the fast decay is attributed to surface trapping of exciton and the slow decay is mainly representative of the radiative processes involving the bound or free excitons. © *2013 American Institute of Physics*.
[http://dx.doi.org/10.1063/1.4774002]

During the past decades, wide band gap semiconductors have attracted a considerable interest for the realization of UV optoelectronic devices. Among the wide bandgap materials, ZnO is an attractive candidate because of its wide bandgap (3.37 eV) and its large exciton binding energy of 60 meV which is sufficient for free excitons to be stable even at room temperature (RT).[1,2] Thus, the excitons play a major role in the optical properties of ZnO. Semiconductor nanoparticles (NPs) with the size in the range of 1–100 nm have attracted great deal of attention because of their unique optical properties and potential for applications in optoelectronics. There are a number of techniques for preparing ZnO NPs, such as vapor phase process, spray pyrolysis, hydrothermal synthesis, and electrochemical growth. Although vapor-phase methods have been extensively used to prepare high optical quality ZnO NPs, the high process temperature above 500 °C limits the substrates available for further applications. Fortunately, ZnO NPs can be synthesized by low-temperature (<300 °C) and low-cost sol-gel methods.[3,4] Recently, light emitting diodes based on ZnO-NPs hybrid structures have been demonstrated.[5,6] Polydisperse aggregated ZnO NPs were used as the electrode material for dye-sensitized solar cells with a high conversion efficiency.[7,8] Colloidal ZnO NPs grown by a sol-gel method have been embedded in a dielectric pillar microcavity by means of radio-frequency sputtering.[9]

To significantly improve their device efficiency and to fully explore their application potential, it is essential to understand the excitonic recombination process in ZnO NPs. From photoluminescence characterization of these quantum dots, information about the inherent material properties, the sensitivity of the material to environmental changes, and the dot structure itself can be gained. There are a number of reports on steady-state photoluminescence studies of the recombination mechanism.[10–14] In order to get more insight on the carrier recombination processes, time-resolved photoluminescence (TRPL) is a powerful tool, because spectral and temporal information can simultaneously be obtained to distinguish different recombination processes. However, very little work has been performed by combining conventional PL with temporal and temperature dependent PL in ZnO NPs.[15,16] Musa *et al.*[15] attributed the defect-related emission around 2.5 eV with a long-lived decay time of several ns to excitons trapped at oxygen vacancies of the dot surfaces. Chernikov *et al.*[16] found that a single fast decay time (<40 ps) of nanoporous ZnO powders is strongly correlated with the appearance of surface-related impurity states in mesoporous samples. However, investigations on the near-band-edge recombination in sol-gel grown ZnO NPs are missing. In this report, an in-depth analysis of exciton recombination processes by time-integrated as well as time-resolved temperature-dependent PL measurements is presented. At room temperature, a blue shift of the free excitonic emission is demonstrated with decreasing particle size as a result of the quantum confinement effect. At low temperatures, the decay time of the bound exciton is concluded to contain two components: the fast one is attributed to the recombination of surface impurities trapped excitons and the slow one is the radiative lifetime of the bound exciton. The thermal evolution of the free and bound exciton recombination is confirmed by temperature dependence of TRPL.

The ZnO NPs were synthesized by a simple sol-gel method. The detail of the synthesis process can be found elsewhere.[3] In brief, the ZnO colloidal solutions were produced from zinc acetate dihydrate (99.5% $Zn(OAc)_2$) in diethylene glycol (99.5% DEG). The reaction solution was heated to 160 °C and maintained for aging in 1 h. After a centrifuge with 6000 rpm to separate the final colloids into the clear suspension and the bottom white powder, the transparent suspension was collected and dropped on a Si substrate. Finally, the product was dried at 250 °C in ambient air for 30 min. The size of ZnO NPs can be varied under a well-controlled concentration of the precursor, $Zn(OAc)_2$ from 0.04 to 0.32 M.

a)Author to whom correspondence should be addressed. Electronic mail: hsuhc@mail.ncku.edu.tw.

The phase and average crystallite size were estimated from x-ray diffraction using a Rigaku 18 kW anode X-ray diffractometer. The morphology was monitored by means of a field emission scanning electron microscope (FE-SEM, Hitachi SU8000). The shapes and sizes of the ZnO NPs were analyzed using a field emission transmission electron microscope (FETEM) operated at 200 keV. Room-temperature micro-photoluminescence (μPL) measurements were performed using a He–Cd laser at 325 nm with an average power of 55 mW. The emission was dispersed by a 0.32 m focal length spectrometer with 1800 grooves/mm grating and detected by a liquid N_2-cooled charged couple device (CCD) detector. For time-resolved micro-photoluminescence (TRμPL) measurements, a frequency triplet mode-locked Ti-sapphire laser at 266 nm with a 150 fs pulse width and 76 MHz repetition rate was employed. The luminescence signal was dispersed by a 0.3 m spectrograph and recorded by a UV sensitive streak camera (Hamamatsu C5680) yielding a spectral resolution of about 1 meV and an overall temporal resolution of 7 ps. The samples were placed in a closed cycle helium cryostat, working in the temperature range T = 5–300 K. For temperature dependent lifetime measurements, we only focus on the largest NPs because the lifetime of the other smaller particles was too short (<7 ps) to observe the temporal dependence with temperature.

Figure 1(a) shows the XRD patterns of the ZnO NPs prepared with various concentrations of $Zn(OAc)_2$. All peaks can be indexed to the hexagonal wurtzite phase of ZnO (JCPDS card No. 36–1451) with lattice constants $a = 0.3251$ nm and $c = 0.5208$ nm. No diffraction peaks from impurities and residues were detected, indicating that the synthesized products are pure ZnO NPs. Although there is no change in the diffraction peak positions, the width of the peaks broadened significantly with decreasing concentration of the precursor. The average crystallite size D can be estimated from the Scherrer formula, $D = 0.89\lambda/\beta \cos\theta$, where λ is the X-ray wavelength (0.15406 nm), θ is the Bragg diffraction angle, and β is the full width at half maximum (FWHM) of the peak diffraction. The calculated particle sizes are 12.8, 9.1, 7.5, and 6.5 nm, for the precursor concentrations of 0.32, 0.16, 0.08, and 0.04 M, respectively. The result is consistent with the observation from TEM as shown in Fig. 1(b).

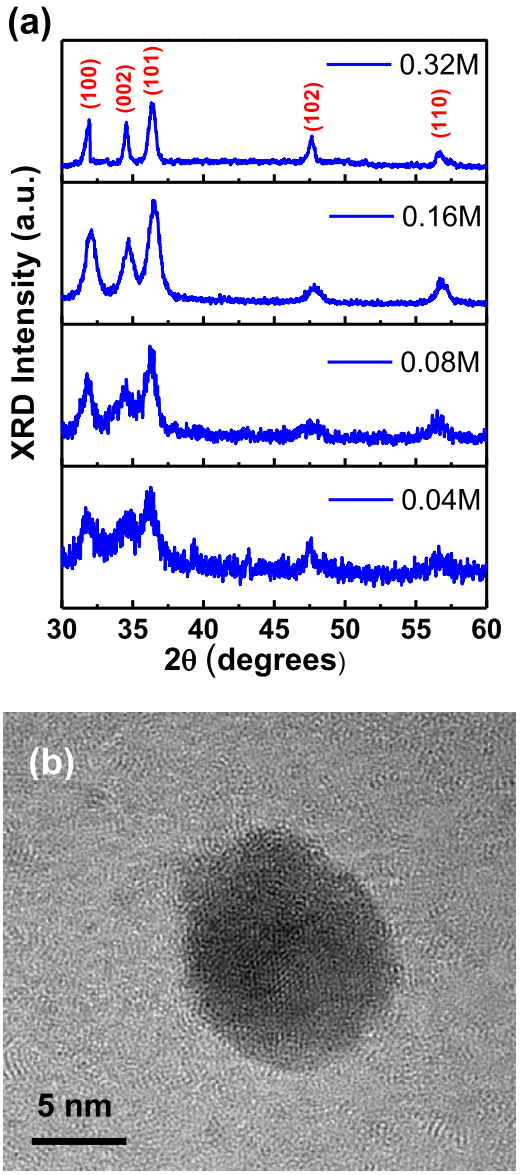

FIG. 1. (a) X-ray diffraction patterns of the ZnO nanoparticles prepared by the sol-gel method, with concentrations 0.32, 0.16, 0.08, and 0.04 M from top to bottom. The crystalline size can be approximately estimated to be 12.8, 9.1, 7.5, and 6.5 nm, respectively. (b) TEM image taken from the product of 0.32 M.

Figure 2(a) shows typical room temperature PL spectra of different sizes of ZnO NPs. Each spectrum consists of a dominant peak in the UV region and a broad peak in the visible. The UV emission is usually ascribed to the free exciton (FX) at the near band edge, as already observed in various ZnO nanostructures.[10] In the case of 12.8 nm ZnO NPs, the FWHM of the UV peak is about 150 meV, which is comparable to the value in previous reports,[13,14] indicating good quality of these NPs. In addition, a weak green emission center at 2.26 eV was observed. Previous investigations have shown that the green luminescence is originating from a free-to-bound recombination between an electron from the conduction band edge with a hole from a trap level or the singly ionized oxygen vacancies at the particle surface have been proposed.[15]

Figure 2(b) shows a blueshift of the FX emission peak as compared to bulk ZnO with decreasing size of the NPs, which is attributed to the quantum confinement effect. In addition, the intensity ratio (in Fig. 2(b)) of the FX emission to the green emission decreases with reduced particle size, which implies that the FX emission is strong for large particles, whereas the green emission dominates for small particles. It can be understood that the increasing surface area to volume ratio for decreasing particle size leads to the predominance of the surface defect-related emission.

To understand the exciton recombination mechanism, the sample of 12.8 nm ZnO NP was selected for extended studies. Figure 3(a) displays the temperature-dependent PL spectra of the 12.8 nm ZnO NP in the temperature range of 10 to 290 K. At 10 K, only one near-band-edge emission centered at 3.382 eV can be observed, which is slightly blueshifted compared to ZnO bulk and nanowires[1,17] due to the quantum confinement effect. In addition, this emission peak is asymmetric, which originates from the recombination of donor-bound excitons ($D^\circ X$) and surface bound exciton

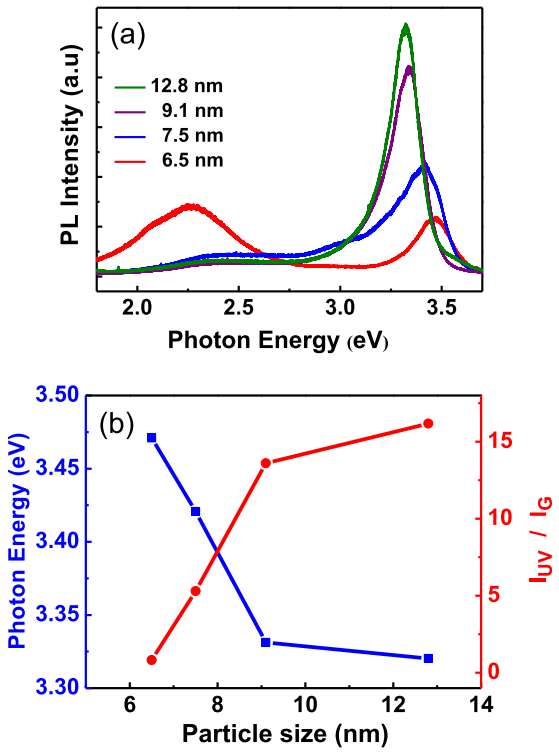

FIG. 2. (a) PL spectra measured at RT of ZnO nanodots of various average diameters. (b) The blue line represents the PL at RT of ZnO nanoparticles of various average diameters. The red line is the ratio of the steady-state PL intensity ratio of the green (G) vs the UV emissions as a function of the size.

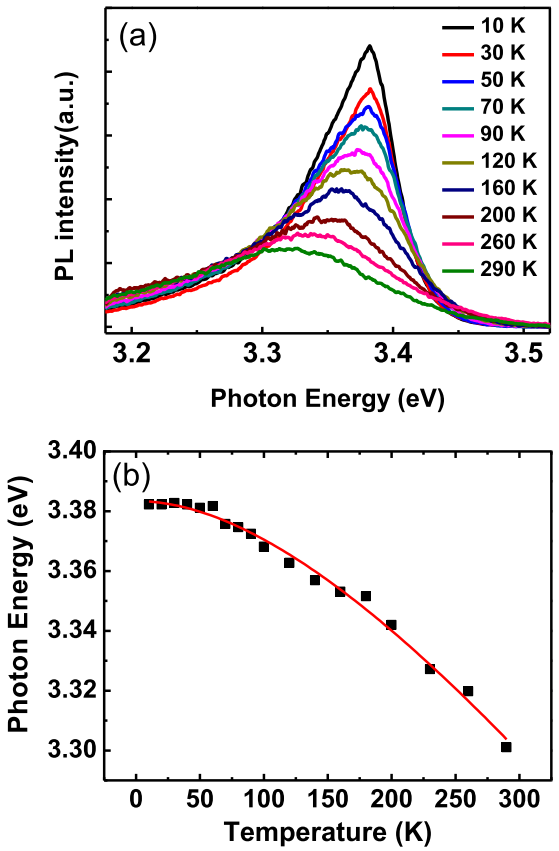

FIG. 3. (a) Temperature dependence of the PL spectra for 12.8 nm ZnO nanoparticles. (b) The solid dots represent the PL peak energy as a function of the temperature for 12.8 nm nanoparticles. The red line is the fitting curve according to the Varshni formula.

emission (SX), as to be discussed below. As the temperature increases, the excitonic emission tends to redshift. The bound exciton emission vanishes at elevated temperatures ($T > 140$ K), while the FX emission appears at high temperatures. This behavior reflects the thermal dissociation of the bound excitons. The variation in peak energy in the temperature range 10–290 K as shown in Fig. 3(b), conforms well to the Varshni formula

$$E_g(T) = E_0 - \frac{\alpha T^2}{T + \beta}, \tag{1}$$

with $E_0 = 3.383$ eV being the transition energy at 0 K, and $\alpha = 6.8 \times 10^{-4}$ eV K^{-1}, $\beta = 428$ K.

Figure 4(a) displays a typical time evolution of the emission spectrum, i.e., a TRPL image of the 12.8 nm ZnO NP at 10 K. The extracted time evolution of the luminescence at 3.371 eV (shown in Fig. 4(b)) exhibits a bi-exponential decay, in agreement with previous reports.[18] Apparently, two different recombination processes are involved in the excitonic

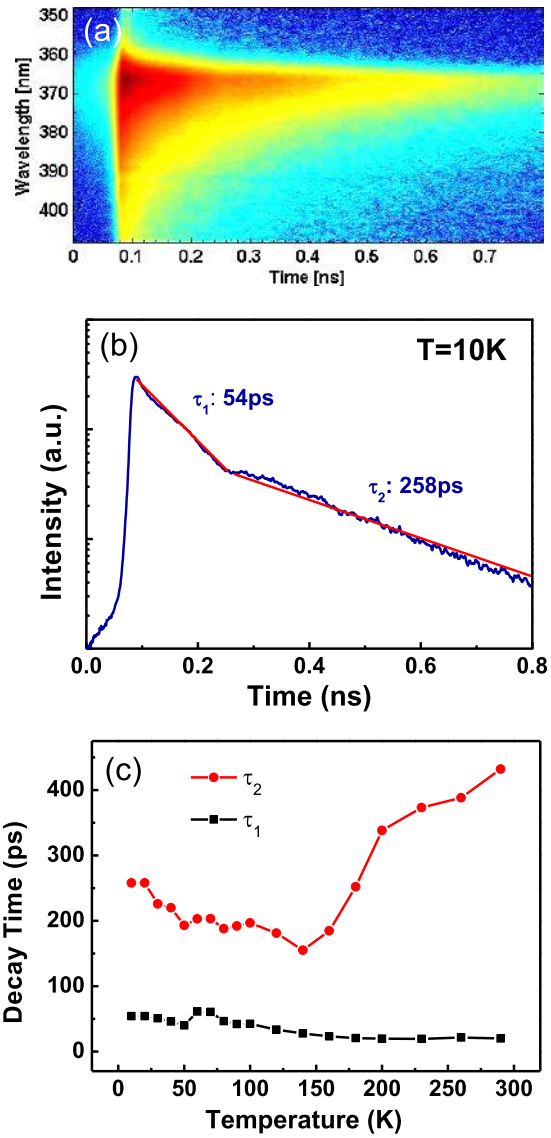

FIG. 4. (a) Time-resolved μPL image showing the time evolution of the PL spectrum at 10 K. (b) Time-resolved μPL spectra measured at the peak energy. The red curve is the result of fitting using two exponential functions. (c) The two decay times as functions of measured temperature.

emission of ZnO at low temperatures. The decay curve was fitted with a bi-exponential function

$$I(t) = A_1 e^{\frac{-t}{\tau_1}} + A_2 e^{\frac{-t}{\tau_2}}, \quad (2)$$

where I(t) represents the PL intensity as a function of time, A_1 and A_2 are the relative weights of the two exponential decays with the time constants τ_1 and τ_2, respectively. The temperature evolutions of the two decay times, $\tau_1 = 54$ ps and $\tau_2 = 258$ ps, are shown in Fig. 4(c).

The existence of two exciton decays with distinctly different lifetimes implies that the emission may occur at different spots. In the study of TRPL on ZnO nanorods, Zhao *et al*. revealed that the fast decay is correlated with the surface related recombination with a decay time increasing with increasing diameter of the nanorods.[19] The asymmetric SX also dominates the near-band-edge PL in ZnO nanorods with diameters $d < 40$ nm.[20] In our case, the surface to volume ratio of the NPs is much larger than for nanorods, and accordingly the surface effect should be obvious in NPs. Theoretical calculations have demonstrated that excitons can be bound to ionized impurities located at the surfaces of quantum dots (QDs).[21] The ultrafast decay dynamics was also observed for ZnO nanocrystals with 8 nm radius due to the SX.[22] Therefore, we believe that the fast decay is correlated with surface trapping of excitons in QDs. Some of the excitons generated within the QDs could diffuse to the surface to become bound by ionized impurities. The trapping time is expected to depend on the impurity density but be independent of temperature. The fast decay time of about 50 ps is almost independent on the temperature revealing that the surface trapping is the predominant decay mechanism. However, the slightly increasing decay rate with temperature could be due to an increasing surface trapping rate with increasing FX velocity as the temperature increases.

On the other hand, the slow decay should be due to the recombination of confined excitons inside the volume of NPs. The decay time represents the radiative lifetime of the free/donor-bound exciton emission. The radiative lifetime of donor bound exciton decreases from 10 K up to 140 K due to a thermally activated increase of the nonradiative decay rate, which is related to the dissociation of the exciton from the donor bound exciton, in agreement with the result of time-integrated photoluminescence. Above 140 K, the bound excitons at localized ionized states are released as free excitons dominate. The radiative lifetime of the free exciton emission is reported to increase with increasing temperature in bulk ZnO.[23,24] The influence of the lattice temperature on the radiative lifetime of the free excitons can be explained simply in terms of an increase in the center of mass kinetic energy. Upon low excitation power level, the free excitons behave as a Maxwell-Boltzmann distribution. Therefore, the exciton redistribution in momentum space changes as lattice temperature increases, giving rise to a successively smaller electron-hole population, which fulfills the momentum conservation requirement for recombination, and hence the radiative recombination lifetime increases with temperature.[25]

In conclusion, the size dependence of the UV photoluminescence spectra of various QD sizes has provided an evidence for the quantum confinement effect. The UV emission near the band edge is attributed to the free exciton emission, and the green emission is originating from surface defects. The temporal behaviors of the excitonic recombination processes of D°X, FX, and SX have been investigated. Our results enrich the current understanding of the recombination dynamics of ZnO nanoparticles and inspire the realization of ZnO-related light emitting devices.

The authors are thankful P. Bergman for providing the time-resolved facilities. This work was financially supported by National Science Council of Taiwan under Grant No. NSC-100-2112 -M-006-002-MY3. This research received funding from the Headquarters of University Advancement at the National Cheng Kung University, which is sponsored by the Ministry of Education, Taiwan.

[1]Ü. Özgür, Y. I. Alivov, C. Liu, A. Teke, M. A. Reshchikov, S. Doğan, V. Avrutin, S.-J. Cho, and H. Morkoç, J. Appl. Phys. **98**, 041301 (2005).
[2]*Zinc Oxide—A Material for Micro- and Optoelectronics Applications*, edited by N. H. Nickel and E. Terukov (Springer, The Netherlands, 2005).
[3]K. F. Lin, H. M. Cheng, H. C. Hsu, L. J. Lin, and W. F. Hsieh, Chem. Phys. Lett. **409**, 208 (2005).
[4]Y. Lin, D. Wang, Q. Zhao, M. Yang, and Q. Zhang, J. Phys. Chem. B **108**, 3202 (2004).
[5]T. Omata, Y. Tani, S. Kobayashi, K. Takahashi, A. Miyanaga, Y. Maeda, and S. Otsuka-Yao-Matsuo, Appl. Phys. Lett. **100**, 061104 (2012).
[6]T. Toyama, H. Takeuchi, D. Yamaguchi, H. Kawasaki, K. Itatani, and H. Okamoto, J. Appl. Phys. **108**, 084302 (2010).
[7]H. M. Cheng and W. F. Hsieh, Energy Environ. Sci. **3**, 442 (2010).
[8]Q. F. Chou, T. R. Chou, B. Russo, S. A. Jenekhe, and G. Z. Cao, Angew. Chem., Int. Ed. **47**, 2402 (2008).
[9]T. Thomay, T. Hanke, M. Tomas, F. Sotier, K. Beha, V. Knittel, M. Kahl, K. M. Whitaker, D. R. Gamelin, A. Leitenstorfer, and R. Bratschitsch, Opt. Express **16**, 9791 (2008).
[10]G. Kiliani, R. Schneider, D. Litvinov, D. Gerthsen, M. Fonin, U. Rudiger, A. Leitenstorfer, and R. Bratschitsch, Opt. Express **19**, 1641 (2011).
[11]Z. D. Fu, Y. S. Cui, S. Y. Zhang, J. Chen, D. P. Yu, S. L. Zhang, L. Niu, and J. Z. Jiang, Appl. Phys. Lett. **90**, 263113 (2007).
[12]K. Suzukia, H. Kondo, M. Inoguchi, N. Tanaka, K. Kageyama, and H. Takagi, Appl. Phys. Lett. **94**, 223103 (2009).
[13]H. Amekura, N. Umeda, Y. Sakuma, N. Kishimoto, and Ch. Buchal, Appl. Phys. Lett. **87**, 013109 (2005).
[14]X. Xiang, X. T. Zu, S. Zhu, Q. M. Wei, C. F. Zhang, K. Sun, and L. M. Wang, Nanotechnology **17**, 2636 (2006).
[15]I. Musa, F. Massuyeau, L. Cario, J. L. Duvail, S. Jobic, P. Deniard, and E. Faulques, Appl. Phys. Lett. **99**, 243107 (2011).
[16]A. Chernikov, S. Horst, T. Waitz, M. Tiemann, and S. Chatterjee, J. Phys. Chem. C **115**, 1375 (2011).
[17]H. C. Hsu, C. S. Cheng, C. C. Chang, S. Yang, C. S. Chang, and W. F. Hsieh, Nanotechnology **16**, 297 (2005).
[18]W. M. Kwok, A. B. Djurišic, Y. H. Leung, W. K. Chan, and D. L. Phillips, Appl. Phys. Lett. **87**, 223111 (2005).
[19]Q. X. Zhao, L. L. Yang, M. Willander, B. E. Sernelius, and P. O. Holtz, J. Appl. Phys. **104**, 073526 (2008).
[20]L. Wischmeier, T. Voss, S. Börner, and W. Schade, Appl. Phys. A **84**, 111 (2006).
[21]V. A. Fonoberov and A. A. Balandin, Appl. Phys. Lett. **85**, 5971 (2004).
[22]G. Pozina, L. L. Yang, Q. X. Zhao, L. Hultman, and P. G. Lagoudakis, Appl. Phys. Lett. **97**, 131909 (2010).
[23]S.-K. Lee, S. L. Chen, D. Hongxing, L. Sun, Z. Chen, W. M. Chen, and I. A. Buyanova, Appl. Phys. Lett. **96**, 083104 (2010).
[24]F. Y. Jen, Y. C. Lu, C. Y. Chen, H. C. Wang, C. C. Yang, B. P. Zhang, and Y. Segawa, Appl. Phys. Lett. **87**, 252117 (2005).
[25]G. E. Bunea, W. D. Herzog, M. S. Ünlü, B. B. Goldberg, and R. J. Molnar, Appl. Phys. Lett. **75**, 838 (1999).